Demonstrating the applicability of chemical looping combustion for the regeneration of fluid catalytic cracking catalysts

Fatih Güleç, Will Meredith, Cheng-Gong Sun, Colin E. Snape

PII: S1385-8947(20)30483-6
DOI: https://doi.org/10.1016/j.cej.2020.124492
Reference: CEJ 124492

To appear in: *Chemical Engineering Journal*

Received Date: 14 October 2019
Revised Date: 10 February 2020
Accepted Date: 17 February 2020

Please cite this article as: F. Güleç, W. Meredith, C-G. Sun, C.E. Snape, Demonstrating the applicability of chemical looping combustion for the regeneration of fluid catalytic cracking catalysts, *Chemical Engineering Journal* (2020), doi: https://doi.org/10.1016/j.cej.2020.124492

Demonstrating the applicability of chemical looping combustion for the regeneration of fluid catalytic cracking catalysts

Fatih Güleç*, Will Meredith, Cheng-Gong Sun, Colin E Snape
University of Nottingham, Faculty of Engineering, Triumph Road, Nottingham NG7 2TU, UK.
*Corresponding author: Fatih.Gulec@nottingham.ac.uk

Abstract

Fluid Catalytic Cracking (FCC) units are responsible for roughly 25 % of CO_2 emissions from oil refineries, which themselves account for 4-6 % of total global CO_2 emissions. Although post- and oxy-combustion technologies have been proposed for CO_2 capture in FCC, Chemical Looping Combustion (CLC) may also be a potential approach that has lower energy consumption. An equilibrium catalyst (ECat) was first modified with oxidised oxygen carriers (CuO, Co_3O_4, Mn_2O_3) using wet-impregnation, and their reduced states (Cu, CoO, Mn_3O_4, MnO) were generated by hydrogen reduction. To demonstrate that the impregnated reduced oxygen carriers had no significant negative effects on cracking, the prepared catalysts were used to crack n-hexadecane using the standard FCC microactivity test (ASTM D3907-13). The CLC behaviour of coke deposited on the reduced oxygen carrier impregnated ECats, was investigated with the stoichiometrically required amount of oxidised oxygen carrier impregnated ECat in lab scale fixed-bed and fluidised-bed reactors equipped with an online mass spectrometer to monitor CO_2 release. Although the conversion and liquid to gas ratio were largely unaffected, coke selectivity did increase with the impregnation of reduced oxygen carriers. However, this increase is mostly attributed to solvent extractable coke. It is possible to reach about 90 vol. % combustion efficiency of the coke deposited on ECat using mechanically mixed with CuO and Mn_2O_3, but the regeneration temperature required, 800 °C, is considerably higher than that under typical regenerator conditions of 650-750 °C for 30-60 min. However, relatively high combustion efficiencies of greater than 94 vol. % of the coke deposited on reduced Cu and Mn_3O_4 impregnated ECat were achieved with the stoichiometrically required amount of CuO and Mn_2O_3 impregnated ECat at 750 °C for 45 min., close to conventional FCC regenerator conditions.

Keywords: CO_2 Capture, Fluid Catalytic Cracking (FCC), Chemical Looping Combustion (CLC), Mn-based oxygen carrier, Cu-based oxygen carrier.

1. Introduction

CO_2 emissions in oil refineries arise from a number of different processes including Fluid Catalytic Cracking (FCC), sulphur recovery and hydrogen production units, in addition to heaters and boilers [1]. The regenerator in a FCC unit is one of the largest CO_2 emitters, contributing about 20-35 % of the total from a standard refinery [1, 2]. Two different CO_2 capture technologies, post-combustion capture (PCC) [3-6] and oxy-combustion capture (OCC) [6-11], have been suggested to mitigate these emissions. The former uses an amine scrubbing technology on the flue gas from regenerator of FCC unit (consisting of 15-20 % of CO_2) [3-6], while in the later highly pure oxygen mixed with recycled CO_2 is used for the combustion of coke in the regenerator instead of air [6-11].

The technical evaluation of PCC and OCC for FCC have demonstrated that the optimum CO_2 capture level for OCC from regenerators in FCC units is about 99 % [6-8], compared to not higher than 90 % for PCC [5-8]. On the other hand, whereas the integration of PCC does not need any major modification of the FCC unit, the regenerator must be modified for OCC technology [12]. However, the stability of operation and the effectiveness of coke combustion [7] during OCC is not compromised, so the operation of OCC-FCC offers potentially a more flexible process than PCC-FCC, requiring a much smaller footprint [6]. In terms of economic evaluation of PCC and OCC for FCC, the total installed cost required for OCC is calculated to be double due to the high air separation unit (ASU) cost compared with that for PCC [7]. The total capital investment for OCC has been estimated at 1.5 times higher than that of PCC [8]. However the chemical cost required for PCC-FCC has been calculated as approximately 80 % higher than that for the OCC-FCC unit. Additionally, while PCC offers lower a capital cost [13], OCC provides a lower CO_2 avoided cost [7, 8].

However, in reality high energy penalties, and the extensive equipment requirements are major problems with both of these technologies. Chemical Looping Combustion (CLC) potentially offers lower energy penalties than PCC [7, 8, 12]. The CLC process, where metal oxides are used as an oxygen supplier instead of air to combust the fuel stream [14, 15], has been suggested as an alternative process to decrease the CO_2 capture cost [15-17]. In CLC, since air and fuel are never mixed [18], the technique does not need any separation process [14, 19, 20] unlike PCC [3-6, 21], or OCC [9, 11, 22].

The applicability of CLC for FCC has been experimentally demonstrated in our previous study [12], with the novel CLC-FCC concept presented in Figure 1. Güleç et al. [12] showed that the mixing of reduced oxygen carriers with equilibrium catalyst (ECat) had no significant impact on the cracking of n-hexadecane. Additionally, greater than 90 % combustion of a model FCC coke was achieved with CuO and Mn_2O_3 at 750 °C for 40-60 min, which is similar to conditions employed in the conventional regenerator of FCC units; 650-750 °C for 30-60 min. However, using mechanically mixing for catalyst preparation introduces heterogeneity of the bed during cracking. Additionally, the TGA results were somewhat constrained by the small amount of model coke used for the CLC tests.

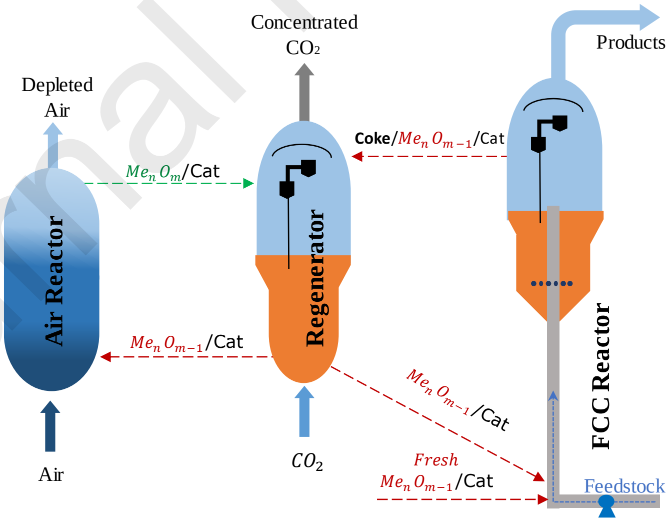

Figure 1. Schematic diagram of the proposed novel CLC-FCC process, (Me_nO_{m-1}/Cat: reduced oxygen carrier impregnated ECat, Me_nO_m/Cat: oxidised oxygen carrier impregnated ECat, Coke/Me_nO_{m-1}/Cat: coke deposited reduced oxygen carrier impregnated ECat) [12].

In this study, the applicability of CLC for FCC is assessed using conditions used in conventional FCC units to provide realistic information on the viability of the overall concept (Figure 1). Reduced oxygen carriers (Cu, CoO, Mn_3O_4 and MnO) were used to modify a commercial FCC catalyst, ECat, via wet-impregnation to compare the results with mechanically mixing, which was used previously [12]. The modified ECats were tested for cracking of n-hexadecane using ASTM D3907-13. Furthermore, the combustion of the coke deposited on the parent ECat and reduced oxygen carrier impregnated ECats were investigated with both bulk oxygen carriers (CuO and Mn_2O_3), and the oxidised oxygen carriers impregnated on the modified ECat (I-CuO/ECat and I-Mn_2O_3/ECat) using lab scale fixed-bed and fluidised-bed reactors at a temperature of *ca.* 750 °C, which is the maximum currently used for FCC regeneration [23].

2. Materials and methods

2.1. Preparation of oxidised and reduced oxygen carrier impregnated ECat

Wet-impregnation was employed for the preparation of modified oxygen carrier ECat. Firstly, a 25 ml aqueous solutions of the required amount of metal nitrate salts, $Cu(NO_3)_2.3H_2O$ (Acros Organics, 99 %), $Co(NO_3)_2.6H_2O$ (Acros Organics, 99 %), and $Mn(NO_3)_2.4H_2O$ (Alfa Aesar, 98 %), were prepared. The amount of oxygen carriers were calculated according to the stoichiometrically required amounts for the combustion of coke deposited on the catalyst. The prepared nitrate solutions were then slowly added to 20 g of ECat, with thorough stirring at room temperature for 18 h. The impregnated samples were then slowly dried at 60 °C for 24 h and 100 °C for 4 h. The dried samples were then calcined at 550 °C for 30 min in an air atmosphere to decompose the impregnated copper nitrate into cupric oxide (CuO), cobalt nitrate into cobalt oxide (Co_3O_4), and manganese nitrate into manganic oxide (Mn_2O_3). The oxidised oxygen carrier impregnated FCC catalysts were then designated as I-CuO/ECat (12.5 wt. % of CuO), I-Co_3O_4/ECat (17.8 wt. % of Co_3O_4), and I-Mn_2O_3/ECat (29.8 wt. % of Mn_2O_3).

To prepare the reduced oxygen carrier impregnated ECats for n-hexadecane cracking, the prepared oxidised oxygen carrier impregnated ECat were reduced using hydrogen in a commercial hydropyrolysis rig [24]. Approximately, 5 g of oxidised oxygen carrier impregnated ECat (I-CuO/ECat, I-Co_3O_4/ECat, and I-Mn_2O_3/ECat) was placed into a stainless steel reactor (9 mm by 25 cm). The reactor was then heated from room temperature to 300 °C (for the reduction of $Mn_2O_3 \rightarrow Mn_3O_4$), 350 °C (for the reduction of $Co_3O_4 \rightarrow CoO$ and $CuO \rightarrow Cu$), 450 °C (for the reduction of $Mn_2O_3 \rightarrow MnO$), with a heating rate of 20 °C/min and kept at the target temperature for 1 h under a hydrogen flowrate of 30 ml/min and a pressure of 5 bar. Then the reduced oxygen carrier impregnated ECats were then designated as I-Cu/ECat, I-CoO/ECat, I-Mn_3O_4/ECat, and I-MnO/ECat.

2.2. Characterization of reduced oxygen carrier impregnated ECat

Both the fresh and used oxygen carrier impregnated ECat were characterized using different techniques to identify potential effects of the modification of the ECat. Crystalline phases were measured using a Siemens D500 X-ray powder diffractometer with Cu-Kα operating at 40 kV and 35 mA. The samples were scanned over a 2θ range of 5° to 55° with a step size of 0.05° and a step time of 2 s. The XRD results were correlated with the references, Joint Committee on Powder Diffraction Standards (JCPDS). The surface morphology, sintering and agglomeration of the modified ECat were scanned at two different magnifications of 100 and 20 µm at 20 kV accelerated voltage using secondary electron imaging (SEI) modes by SEM (JEOL JSM 6490LV). The textural properties of the oxygen carrier impregnated ECat catalysts derived from nitrogen sorption measurements were conducted using Micrometrics ASAP 2420 (Accelerated Surface Area and Porosimetry System) N_2 sorption instrument. The percentage of impregnated oxygen carrier on ECat was quantitatively measured by X-ray fluorescence (XRF) using Panalytical Epsilon 3-XL. The Brönsted and Lewis acidities of the catalysts were measured by Pyridine-Fourier-transform infrared spectroscopy (Py-IR). The contents of coke (carbon and hydrogen) on the catalysts were quantified by elemental analysis using a Leco CHN628 analyser. The true density of reduced oxygen carriers impregnated ECat were measured by a Micromeritics AccuPyc II 1340 Gas Pycnometer.

2.3. Cracking activity of reduced oxygen carrier impregnated ECat

The cracking activity of reduced oxygen carrier impregnated ECats; I-Cu/ECat, I-CoO/ECat, I-MnO/ECat, and I-Mn_3O_4/ECat, were investigated using a microactivity test (MAT) unit (Figure 2) using ASTM D3907 [25], the standard method for testing of FCC catalysts. The cracking experiments were performed as described previously [12]. Briefly, the reactor containing 4 g of ECat (with the impregnated reduced oxygen carrier) was placed in a tubular furnace, and the temperature was then increased to 482 °C (± 5 °C) with a heating rate of 20 °C/min, under an N_2 flow of 20 ml/min. The reactor was purged with N_2 for 30 min at 482 °C. After 1.33 g of n-hexadecane injection for 75 s into MAT reactor was completed, both MAT reactor and liquid product receiver was purged with an N_2 flow of 20 ml/min for 15 min. The liquid cracking products were condensed using a water-ice bath and collected with a liquid product receiver. Additionally, the gas products were collected in a 1-litre gas bag. To reduce experimental error, the cracking tests were repeated three times with fresh catalysts for each test, and the conversion, yields and selectivities are presented with error bars representing one standard deviation. The liquid and gas products were analysed using a Clarus 580 GC (Perkin Elmer Elite-1 phase 60 m x 0.25 mm x 0.25 µm capillary column) fitted with TCD and FID detectors.

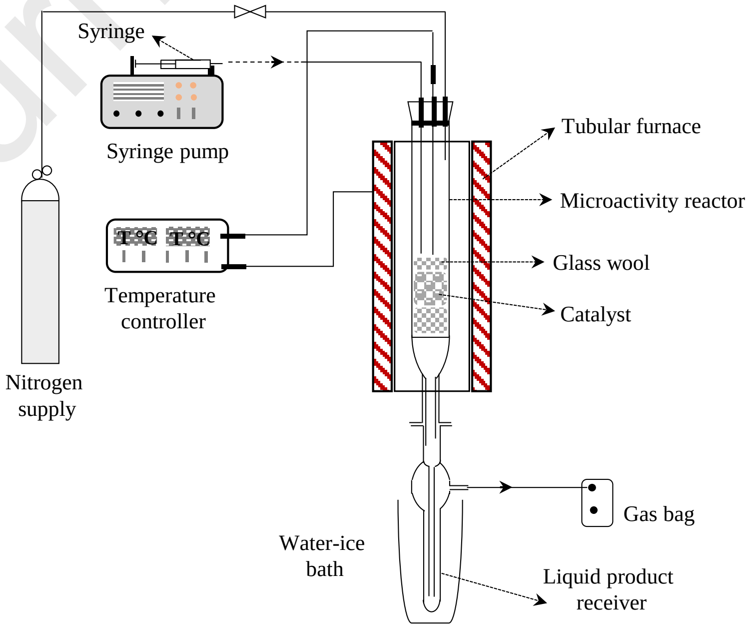

Figure 2. The experimental configuration of the MAT unit [12, 25].

Conversions of n-hexadecane (E1 and 2) to coke, liquid, and gas (E3, 4 and 5) and product selectivities (E 6) to C_{1-2} (dry gas), C_{3-4} (LPG), C_{5-15} (gasoline), C_{16+} (higher hydrocarbons) were determined as previously described [12].

$$\text{Conversion (overall) wt.\%} = \frac{W_{C16,0} - W_{C16,f}}{W_{C16,0}} * 100 \qquad \text{(E1)}$$

$$\text{Conversion (excluding CLC) wt.\%} = \frac{W_{C16,0} - (W_{C16,f} + W_{CO_2})}{W_{C16,0}} * 100 \qquad \text{(E2)}$$

$W_{C16,0}$: The weight of n-hexadecane feed (g), $W_{C16,f}$: The weight of uncracked n-hexadecane in the products (g), W_{CO2}: Total weight of carbon in carbon dioxide in the products (g).

$$\text{Gas yield} = \frac{W_g}{W_{C16,0}} * 100 \qquad \text{(E3)}$$

$$\text{Coke yield} = \frac{W_C}{W_{C16,0}} * 100 \qquad \text{(E4)}$$

$$\text{Liquid yield} = \frac{(W_{C16,0} - W_{C16,f} - W_g - W_C)}{W_{C16,0}} * 100 \qquad \text{(E5)}$$

$W_{C16,0}$: The weight of n-hexadecane feed (g), $W_{C16,f}$: The weight of uncracked n-hexadecane in the products (g), W_g: Total weight of gas products (g), W_C: Total weight of coke (g).

$$\text{Selectivity of i (wt.\%)} = \frac{W_i}{\sum W_{\text{products}}} * 100 \qquad \text{(E6)}$$

W_i: The weight of i product (C_{1-2} (dry gas), C_{3-4} (LPG), C_{5-15} (gasoline), C_{16+} (higher hydrocarbons) and coke), g. $\sum W_{\text{products}}$: Total weight of the products C_{1-2}, C_{3-4}, C_{5-15}, C_{16+}, and Coke, g.

2.4. CLC tests of FCC coke with oxygen carriers

CLC tests of coke deposited on ECat with bulk CuO and Mn_2O_3:

The CLC tests of the coke deposited on ECat with bulk CuO and Mn_2O_3 was investigated using a lab-scale fixed-bed reactor equipped with an online mass spectrometer (FxB-MS, Figure 3) unit. ~0.92 g of coke deposited ECat (containing 4.55 wt. % C) was firstly mixed with the stoichiometrically required amount of bulk CuO (~1.38 g) and bulk Mn_2O_3 (3.79 g). The mixture was then placed in a quartz reactor located in tubular furnace, heated from ambient temperature to the combustion temperature, 800 °C, with a heating rate of 20 °C/min under a N_2 flow rate of 35 ml/min and the temperature was kept at this level until the combustion finished. The CO_2 released from the combustion of coke were screened by an on-line mass spectrometer.

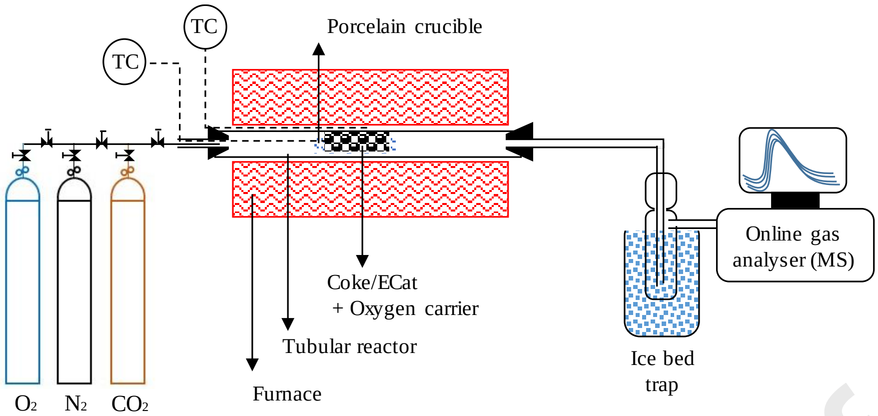

Figure 3. Schematic diagram of the FxB-MS experimental set-up.

CLC tests of coke deposited on reduced oxygen carrier ECat with oxidised oxygen carriers impregnated ECat in FxB-MS and FsB-MS units:

To investigate the combustion of coke deposited on reduced oxygen carrier ECat (I-Cu/ECat and I-Mn_3O_4/ECat) with oxidised oxygen carriers impregnated ECat (I-CuO/ECat and I-Mn_2O_3/ECat), as in the proposed CLC-FCC concept, the CLC tests were investigated using the lab-scale FxB-MS and FsB-MS (fluidised-bed reactor equipped with an online gas analyser, Figure 4).

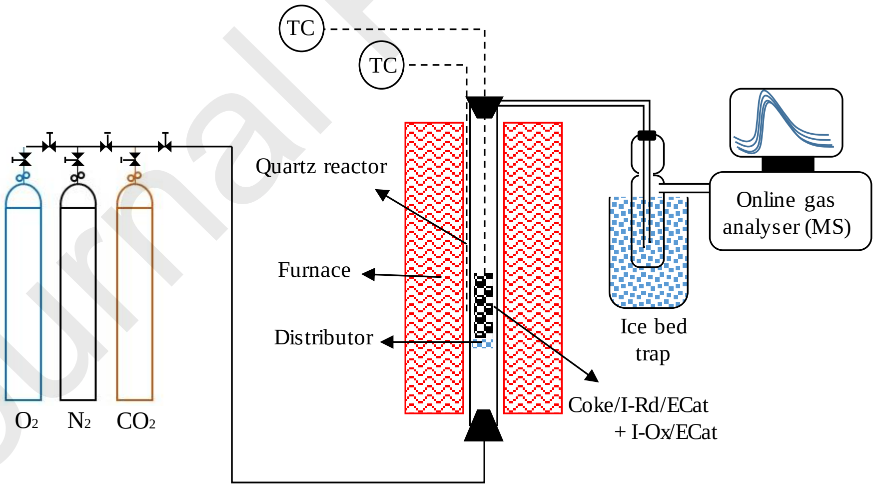

Figure 4. Schematic diagram of FsB-MS experimental set-up (Rd: reduced oxygen carrier, Ox: Oxidised oxygen carrier).

For the CLC tests in the FxB-MS, ~1.85 g coke deposited I-Cu/ECat (0.939 wt. % of C and 0.062 wt. % of H) was mixed with ~4.64 g of I-CuO/ECat (0.56 g of CuO) and ~1.85 g coke deposited I-Mn_3O_4/ECat (0.949 wt. % of C and 0.097 wt. % of H) was mixed with ~6.24 g of I-Mn_2O_3/ECat (1.81 g of Mn_2O_3).

The mixtures were placed in a quartz reactor located in horizontal tube furnace, shown in Figure 3, heated from ambient temperature to the combustion temperature, 750 °C and 800 °C, with a heating rate of 20 °C/min under a N_2 flow rate of 35 ml/min and the temperature was kept at this level until the combustion finished. For the CLC tests in FsB-MS, the combustion of coke deposited on I-Cu/ECat and I-Mn_3O_4/ECat with I-CuO/ECat and I-Mn_2O_3/ECat were investigated using the minimum fluidisation velocity (U/U_{mf} = 1.0). The mixture was placed in a quartz fluidised bed reactor and placed into the tubular furnace, the flow rate was set to the minimum fluidisation flow rate of N_2 (280 ml N_2/min). The reactor was then heated from room temperature to 750 °C, with a heating rate of 20 °C/min under a N_2 flow rate of minimum fluidisation velocity and the temperature was kept at this level until the combustion finished.

Calibration graph for converting ion current to the volume percent of CO_2 in combustion gases:

To present the combustion results measured by the MS in a comprehensible manner, a calibration graph was drawn of ion current vs the volumetric ratio of CO_2 and presented in Figure B1 (Appendix B). A group of gas mixtures having different volumetric ratios of CO_2 and N_2 were prepared and analysed in MS to get the specific ion current (A) values for the specific ratio of CO_2 mixtures. Each gas mixture containing a different volumetric ratio of CO_2 had a specific ion current value.

The combustion % for all these CLC tests was calculated using Equation 7 in volume based.

$$\text{Combustion (vol. \%)} = \frac{V_{CO_{2,MS}}}{V_{CO_{2,Coke}}} * 100 \qquad \text{(E7)}$$

$V_{CO_{2,MS}}$: Volume of CO_2 measured by MS during the combustion of coke with oxygen carrier (ml). $V_{CO_{2,Coke}}$: Volume of CO_2 calculated on the basis of carbon in the coke (ml).

3. Results and discussion

3.1. Characterization of reduced oxygen carriers impregnated ECat

X-ray diffraction (XRD) analysis:

The XRD patterns of both fresh and used reduced oxygen carrier impregnated ECat, I-Cu/ECat, I-CoO/ECat, I-Mn_3O_4/ECat, and I-MnO/ECat, are presented in Figure A1 in Appendix A. As shown, the characteristic ECat peaks, indicated with black stars (from $2\theta = 5°$ to $32°$), remain after the reduction of the fresh oxygen carrier impregnated ECats by hydrogen (pattern 2). Further, the characteristic ECat peaks also remain after the reduced oxygen carrier impregnated ECat was tested following the cracking of n-hexadecane (pattern 3). Additionally, the catalysts, I-Cu/ECat and I-MnO/ECat, did not show any deformation after either reduction (patterns -a2 and -b2) or cracking (patterns -a3 and -b3). A further reduction of unreduced Co_3O_4 (in I-CoO/ECat) and Mn_2O_3 (in I-Mn_3O_4/ECat) to the CoO-Co and Mn_3O_4-MnO states were observed after n-hexadecane cracking, as demonstrated in Figure A1-c3 and -d3. However, due to the small portion of oxidised states in reduced oxygen carrier impregnated ECat, it would not impact on the effectiveness of cracking.

X-ray fluorescence (XRF) analysis:

The percentage of the reduced oxygen carriers, Cu, CoO, Mn_3O_4 and MnO, impregnated on ECat, and the true densities of the prepared catalysts are presented in Table A1 in Appendix A. The true density of the ECat slightly increased with the modification by reduced oxygen carriers as the densities of Cu (8.92 g/cm^3), CoO (6.44 g/cm^3), Mn_3O_4 (4.86 g/cm^3) and MnO (5.43 g/cm^3) are higher than the density of ECat (2.70 g/cm^3). However, due to the low percentage of impregnated reduced oxygen carriers, the increase in the true densities of ECat was relatively low. The XRF results prove that the required amount of reduced oxygen carriers were successfully impregnated on the ECat, which are *ca*. 5.4 wt. % of Cu, 16.3 wt. % of CoO, 29.4 wt. % of Mn_3O_4, and 26.7 wt. % of MnO.

Scanning electron microscope (SEM) analysis:

The SEM images (Figure A2 in Appendix A) demonstrate that no agglomeration was observed on I-Cu/ECat or I-CoO/ECat after reduction by hydrogen. However, the others (I-MnO/ECat and I-Mn_3O_4/ECat) did demonstrate some agglomeration between catalyst particles after impregnation. In addition, while I-Cu/ECat did not show any fragmentation after reduction or cracking, the others did show some fragmentation. This was thought to be due to the oxidised oxygen carrier impregnation process rather than the reduction with hydrogen or the cracking. Additionally, metal (Cu-, Co-, Mn-) accumulation on the catalyst surface was clearly observed by SEM images (Figure A2).

N_2 adsorption-desorption analysis:

The nitrogen sorption isotherms and textural properties of reduced oxygen carrier modified ECat, I-Cu/ECat, I-CoO/ECat, I-Mn_3O_4/ECat, and I-MnO/ECat, are presented in Figure A3 and Table A2. Impregnation of reduced oxygen carriers did not change the form of the sorption isotherms of the ECats, which are defined as “type IV” according to International Union of Pure and Applied Chemistry (IUPAC) classification [26, 27]. After the impregnation of the reduced oxygen carriers, a decrease on BET surface area was observed, approximately 12 m^2/g for the impregnation of Cu, CoO, MnO and about 22 m^2/g for the impregnation of Mn_3O_4. The decrease in the surface area by the impregnation of metals may be attributed to pore blocking by the metals impregnated pore mouths. However, as will be described, the fact that cracking activity remains high indicates that access to the zeolite micropores is not significantly affected In terms of pore volume, the reduced oxygen carriers impregnated ECat demonstrated a similar total pore volume around 0.19 cm^3/g that was slightly lower than the parent ECat (0.25 cm^3/g). As for the average pore diameter, the impregnation of Cu and Mn_3O_4 slightly decreased it whereas the impregnation of MnO and CoO had no significant effect. Furthermore, the neck diameter was not affected by the impregnation of Cu, CoO or MnO. The decrease in surface area, pore volume and pore diameter may be attributed to the diffusion of oxygen carriers into the ECat pores. As decreasing trend in BET surface area and pore volume with the modification of transition metals on zeolite catalysts have been observed previously [28-32].

Acidity via Fourier-transform infrared spectroscopy of pyridine adsorption (Py-IR):

The Brönsted (B) and Lewis (L) acidities measured by Py-IR of parent ECat and reduced oxygen carriers impregnated ECat, I-Cu/ECat, I-CoO/ECat, I-Mn_3O_4/ECat, and I-MnO/ECat, are presented in Figure A4 and the integrated area of the peaks are summarized in Table A3 using arbitrary units. The intensity of Lewis acid sites at around 1445 cm^{-1} were considerably higher than that of Brönsted acid sites at about 1540 cm^{-1} for the parent and reduced oxygen carrier impregnated ECat. Additionally, both Lewis and Brönsted acid sites demonstrated a decrease with the impregnation of reduced oxygen carriers, which are in line with previous studies [31, 33]. The decrease in the acid sites may be attributed to the decrease in the surface area and pore volume due to the impregnation of oxygen carriers.

3.2. Catalytic cracking activity of the reduced oxygen carriers impregnated ECat

The cracking activity of the reduced oxygen carrier impregnated ECats was investigated using n-hexadecane, with the total conversion (overall and excluding-CLC), coke, gas, liquid yields, and product selectivities presented in Figures 5, 6 & 7, respectively. The negligible increases in the overall conversion, where CLC was included arise from the very small amounts of C in the CO_2 produced by the combustion reaction during the cracking reactions.

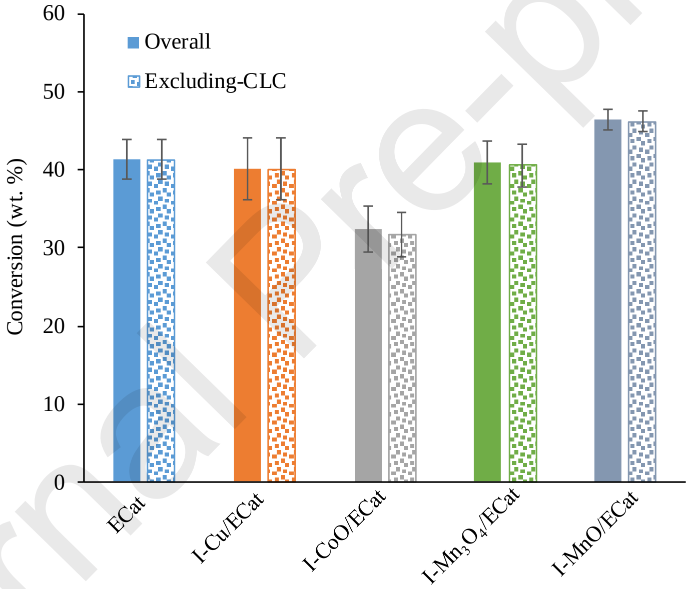

Figure 5. Conversion (overall and excluding CLC) of n-hexadecane over the control ECat and reduced oxygen carriers impregnated ECat; I-Cu/ECat, I-CoO/ECat, I-Mn_3O_4/ECat, and I-MnO/ECat.

Figure 5 shows that there were no significant differences between the overall conversion and that excluding CLC for the reduced oxygen carrier impregnated ECat, which implies that there was no further reduction of reduced oxygen carriers due to the combustion of the cracking feed (n-hexadecane or cracked products) has occurred, which is confirmed by the XRD patterns of the used catalysts (Figure A1). However, in our previous research [34], we demonstrated that the selective CLC of higher alkanes (n-hexadecane and n-heptane) with oxidised oxygen carriers such as CuO and Mn_2O_3 is possible. Thus, determining the state of oxygen carriers (oxidised or reduced) is essential to eliminate combustion during cracking in the riser with the oxygen carrier modified catalysts. In contrast to earlier studies demonstrating a negative impact of Cu impregnation on the effectiveness of ZSM-5 for the cracking of palm oil, attributed to a decrease of the Brönsted acidity [35], the conversion of n-hexadecane here was not affected by the impregnation of Cu or Mn_3O_4. Although reduced, the Brönsted acidity remaining after Cu or Mn_3O_4 impregnation (Table A3) is still sufficient for cracking n-hexadecane [28]. For CoO impregnation which caused a dramatic reduction in the amount Brönsted acidity, the conversion of n-hexadecane was found to decrease to about 32 wt. %. However, both the pore structure and acidity remained at a similar level after impregnation with MnO (Table A3 in Appendix A).

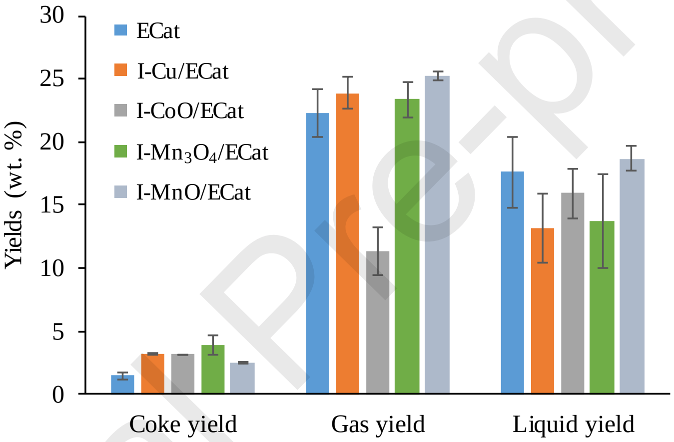

Figure 6. Coke, gas, and liquid yields from the cracking of n-hexadecane over the initial ECat and after reduced form oxygen carrier impregnation ECat; I-Cu/ECat, I-CoO/ECat, I-Mn_3O_4/ECat, and I-MnO/ECat.

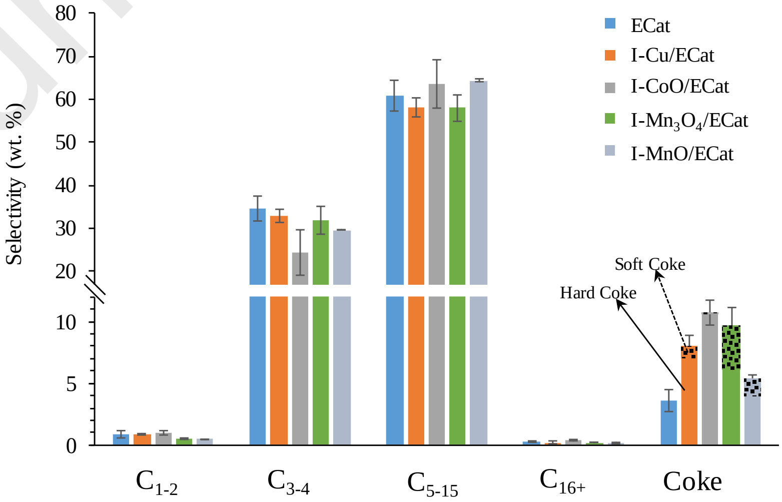

Figure 7. Product selectivity of C_{1-2} (light gases), C_{3-4} (LPG), C_{5-15} (gasoline), C_{16+} (higher hydrocarbons) and coke from the cracking of n-hexadecane over the initial ECat and reduced oxygen carriers impregnated ECat; I-Cu/ECat, I-CoO/ECat, I-Mn_3O_4/ECat, and I-MnO/ECat.

Figure 6 shows that the coke yield increase from 1.5 wt. % to about 3.0 wt. % with the impregnation of Cu and CoO, to 2.5 wt. % with the impregnation of MnO, whereas the impregnation of Mn_3O_4 almost trebled the coke yield, which may be attributed to the constriction of pore structure. Although the coke yields did increase with the impregnation of reduced oxygen carriers, the liquid to gas ratios were largely unaffected (except for the impregnation of CoO). Similarly, the increase in the coke deposition on the FCC catalyst modified with MnO_3 after cracking of cumene was demonstrated by Hosseinpour et al. [36]. Although the impregnation of Cu decreased the coke deposition during the cracking of bio-oil, overloading of Cu increased the coke deposition [37]. The coke increase was attributed to the Lewis acid sites, which could promote the coking and results in deactivation due to the dehydrogenation reaction to the produce coke precursors [37].

As for the gas and liquid yields, while the impregnation with CoO reduced the gas yield by about half, the other reduced oxygen carriers did not appear to impact the gas or liquids yields to any great extent. Excluding coke formation, the use of reduced oxygen carrier modified ECat on the product selectivity was insignificant (Figure 7) except for the selectivity of LPG over CoO impregnated ECat, which may also explain the lower gas yield as presented in Figure 6. Given that the reduced oxygen carriers increased the coke yield on the catalyst, identification of the coke structure (soft coke and hard coke, Table-1) on the catalyst after the modification with the reduced oxygen carriers is, therefore, an important issue for the proposed CLC-FCC concept.

Table 1. Coke percentage and normalized coke composition of used catalysts; ECat, I-Cu/ECat, I-CoO/ECat, I-Mn_3O_4/ECat, I-MnO/ECat.

Catalyst	**Coke on catalyst[a] (wt. %)**		**Coke composition[b] (wt. %)**		**Coke type (wt. %)**		**H/C[e]**
	Carbon	**Hydrogen**	**Carbon**	**Hydrogen**	**SC[d]**	**HC[c]**	
ECat	0.45 ±0.02	0.03 ±0.01	93.6 ±2.2	6.4 ±2.2	0.5	99.5	0.80
I-Cu/ECat	1.09 ±0.34	0.09 ±0.01	91.9 ±2.3	8.1 ±2.3	8.4	91.6	0.99
I-CoO/ECat	1.00 ±0.15	0.05 ±0.07	95.1 ±0.9	4.9 ±0.9	0.6	99.4	0.60
I-Mn_3O_4/ECat	1.22 ±0.16	0.09 ±0.05	93.6 ±2.7	6.4 ±2.7	32.8	67.2	0.88
I-MnO/ECat	0.77 ±0.01	0.05 ±0.01	93.1 ±0.9	6.9 ±0.9	19.5	80.5	0.78

[a] Based on g of total coke/ g of ECat. [b] Normalized coke composition was calculated by (weight of carbon (or hydrogen) / weight of coke)*100, wt. %. [c] Hard Coke, the remain coke % after solvent extraction. [d] Soft Coke was determined using the differences of (100-HC), wt. %. [e] The ratio of H/C was calculated as the weight of H*12/weight of C.

Coke analysis:

In general, being formed by the cracking reactions over the catalysts, coke also arise from thermal and metal-mediated reactions, which can contribute the overall level of coke on the catalysts [38]. Therefore, the increase in the coke yield for impregnation compared to physical mixing [12] gives small reductions in surface area (Table A2) consistent with the relatively small increases in coke yield (Table 1). In terms of the pore structure, an inverse relationship between average pore diameter (Table A2) and coke deposition was obtained for the reduced oxygen carrier impregnated ECat, as the average pore diameter followed the trends ECat > I-MnO/ECat > I-CoO/ECat > I-Cu/ECat > I-Mn_3O_4/ECat while the carbon percentage on catalysts displayed the opposite trend. The highest level of coke (1.22 wt. % C) was found on I-Mn_3O_4/ECat which had the lowest average pore diameter of 12.8 nm and neck diameter of 8.8 nm once compared with other reduced oxygen carriers impregnated ECat. As mentioned previously, a clear decrease in the surface area was observed due to the pore blockage after the impregnation of CuO, Co3O4 and Mn2O3, which slightly changed the matrix structure of ECat. Koon et al. [38] proved that after the extractable soft coke removed from the catalysts structure, a further pool of soft coke was found as physically entrapped within the catalyst pore structures and it was only released after demineralisation. Additionally, this second soft coke contains more aromatics, which ultimately controls the final coke yield. The further coke formation may be attributed to the decrease in the effective pore diameter and increase in the diffusion resistance of reactants/products in the modified ECat catalysts.

Additionally, the differences of the soft and hard coke rations (Table 1 and Figure 7) may be attributed to the metal-mediated coke formation reactions. As each type of metals impregnated on ECat differently promoted the coke formation reactions. For example, after Mn- based reduced oxygen carrier modification, a dramatic increase in the soft coke was observed (Table 1), which also arise the total coke ratio on the catalyst. However, the coke calculated for the reduced oxygen carriers impregnated ECat was in the range reported in the literature where the FCC catalysts contain 0.46-1.74 % of insoluble coke

[39] having a H/C ratio of 0.27-0.54. The expected coke was also about 0.8-1.0 wt. % according to the figure drawn for the cracking time versus carbon deposition by Alexis Voorhies [40]. As for the hydrogen content, it was slightly higher due to the moisture content of the catalysts of 2-4 wt. % [39].

As for the catalyst deactivation by coke deposition, Koon et al [38] demonstrated that significant variations occur in the structure of both hard and soft coke during stripping of coke deposited ECat by the cracking of low sulphur vacuum gas oils (VGO). Although the hard coke becomes more highly condensed with prolonged stripping, the surface area reduction by the hard coke remains fairly constant for stripping periods in excess of ca. 5-10 minutes and is very small, 10 m^2/g.

3.3. CLC tests of coke with Cu- and Mn-based oxygen carriers in FxB-MS and FsB-MS units

CLOU properties of oxidised oxygen carrier impregnated ECats:

The chemical looping with oxygen uncoupling (CLOU) properties of I-CuO/ECat and I-Mn_2O_3/ECat were investigated and compared with those of bulk CuO and Mn_2O_3, respectively. Figure 8-a demonstrates that oxygen release started at ~520 °C, and linearly increased with temperature until ~740 °C, after which the rate of oxygen release increased rapidly. However, when the same amount of bulk CuO was tested, oxygen release started at ~780 °C, and the rate was constant until 800 °C. These tests substantiate previous findings [19, 41, 42] in which the auto-decomposition of CuO to Cu_2O starts at ~790 °C. As with I-CuO/ECat, the impregnation of Mn_2O_3 on ECat clearly enhanced the CLOU properties of Mn_2O_3 at the lower temperatures (Figure 8-b).

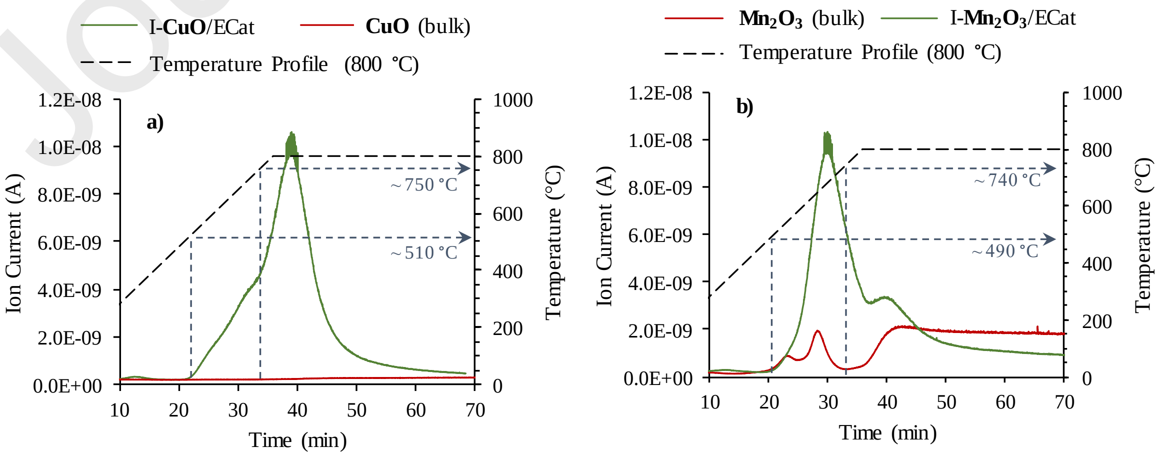

Figure 8. Comparison of chemical looping oxygen uncoupling properties of bulk CuO and I-CuO/ECat, b) bulk Mn_2O_3 and I- Mn_2O_3/ECat, at 800 °C under N_2 atmosphere in FxB-MS unit.

The impregnation of CuO and Mn_2O_3 onto the ECat clearly enhanced the oxygen releasing properties at lower temperatures, which may be attributed to the dispersion of CuO and Mn_2O_3 on the catalyst surface, which acts as a support for the oxidised oxygen carriers impregnated ECat in the regenerator.

CLC tests of coke deposited on reduced oxygen carrier impregnated ECat with oxidised oxygen carriers impregnated ECat in FxB-MS and FsB-MS units:

As suggested in the proposed CLC-FCC unit, it is important to identify the combustion behaviour of coke deposited on reduced oxygen carrier impregnated ECat (coming from the FCC riser) combined with the oxidised oxygen (coming from the air reactor). Therefore, the coke deposited on I-Cu/ECat and I-Mn_3O_4/ECat during the cracking of n-hexadecane was combusted using their oxidised states with impregnated ECat catalysts, I-CuO/ECat and I-Mn_2O_3/ECat, respectively. The coke deposited on I-CoO/ECat was not investigated due to its detrimental effect on cracking described above.

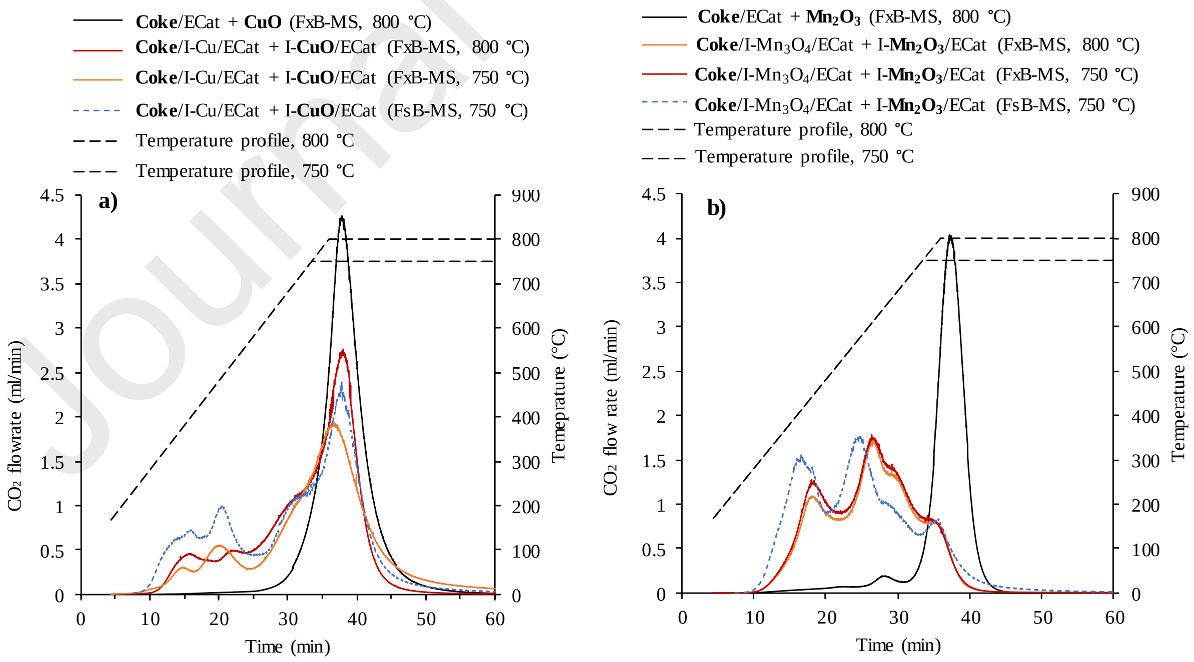

Figure 9. Combustion results of coke deposited on a) I-Cu/ECat with I-CuO/ECat, and b) I-Mn_3O_4/ECat with I-Mn_2O_3/ECat, at 800 and 750 °C under N_2 atmosphere in FxB-MS and FsB-MS units and the comparison with the combustion of coke deposited ECat with bulk CuO and Mn_2O_3 at 800 °C in FxB-MS unit (FxB: Fixed bed, FsB: Fluidised bed, MS: Mass spectroscopy).

The CO_2 evolution for the combustion of coke deposited on I-Cu/ECat demonstrated three main parts, as shown in Figure 9-a. The first part (290-560 °C) may be attributed to the combustion of soft coke with solid CuO impregnated on ECat, while the second and third parts (560-740 °C and 740 °C <) are a consequence of the combustion of hard coke with gas phase oxygen released from I-CuO/ECat. Furthermore, in the FsB-MS unit under a minimum fluidisation velocity, the CO_2 evolution shifted to lower temperatures where the soft coke combustion started at about 250 °C but hard coke combustion started at 560 °C as it was on FxB-MS unit. Table 2 shows that the combustion of coke deposited on I-Cu/ECat with I-CuO/ECat reached 98 vol. % and 88 vol. % at the temperatures of 800 and 750 °C respectively in the FxB-MS unit for 45 min. Furthermore, the combustion was found to increase from 88 vol. % to 96 vol. % at 750 °C for 45 min when the FsB-MS unit used instead of FxB-MS unit.

Due to the combustion of the soft coke (32.8 wt. %, Table 1), the combustion of coke deposited on I-Mn_3O_4/ECat with I-Mn_2O_3/ECat started at about 290 °C in FxB-MS unit (Figure 9-b). The combustion of hard coke was shifted to a lower temperature of 510 °C thanks to the oxygen released from I-Mn_2O_3/ECat (demonstrated in Figure 8-b). When the test was repeated in FsB-MS, the CO_2 evolution was shifted to lower temperatures where the soft coke combustion started at about 250 °C and hard coke combustion started at 490 °C.

Table 2. Combustion % of coke deposited on I-Cu/ECat with I-CuO/ECat, and I-Mn_3O_4/ECat with I-Mn_2O_3/ECat, at 800 and 750 °C under N_2 atmosphere in FxB-MS and FsB-MS units and the comparison with the combustion of coke deposited ECat with bulk CuO at 800 °C in FxB-MS unit.

Coke source	**Oxygen carrier**	**Reactor**	**Temperature**[c] **(°C)**	**$V_{CO2,Coke}$**[d] **(ml)**	**$V_{CO2,MS}$**[e] **(ml)**	**Combustion (vol. %)**
Coke/ECat [a]	**CuO** (bulk)	Fixed	800	27.7	27.2	98
Coke/I-Cu/ECat [b]	I-**CuO**/ECat	Fixed	800	29.9	29.2	98
Coke/I-Cu/ECat [b]	I-**CuO**/ECat	Fixed	750	30.1	26.4	88
Coke/I-Cu/ECat [b]	I-**CuO**/ECat	Fluidised	750	33.1	31.8	96
Coke/ECat [a]	**Mn_2O_3** (bulk)	Fixed	800	20.7	19.3	93
Coke/I-**Mn_3O_4**/ECat [b]	I- **Mn_2O_3**/ECat	Fixed	800	26.1	24.0	92
Coke/I-**Mn_3O_4**/ECat [b]	I- **Mn_2O_3**/ECat	Fixed	750	29.9	25.6	87
Coke/I-**Mn_3O_4**/ECat [b]	I- **Mn_2O_3**/ECat	Fluidised	750	33.1	31.1	94

[a] Coke deposited on ECat during cracking reaction of n-hexadecane. [b] Coke deposited on I-Cu/ECat or I-Mn_3O_4/ECat during the cracking reaction of n-hexadecane. [c] Combustion temperature. [d] Volume of CO_2 calculated on the basis of carbon in coke measured by LECO. [e] Volume of CO_2 calculated by the integration of the graph presented in Figure 11 for 45 min (between 5-50 min).

Combustion behaviour of coke with air, bulk-CuO and I-CuO/ECat:

The combustion behaviour of coke with air, bulk-CuO and CuO impregnated ECat (I-CuO/ECat) are compared in Figure 10. The combustion of coke with air started at about 350 °C, reached a maximum level at 700 °C and completed in 25 min. Although the combustion of coke with bulk CuO reached a reasonably high value (93 vol. %) at the temperature of 750 °C for 45 min, it started at a much higher temperature than with air. On the other hand, using CuO impregnated ECat (I-CuO/ECat) as the oxygen supplier, the combustion of coke started at lower temperatures than with bulk-CuO as already clarified. The extent combustion reached 96 vol. % at 750 °C for 45 min thanks to the enhancement on CLOU properties of CuO after impregnated on the ECat. Furthermore, complete combustion was achieved compared with bulk CuO.

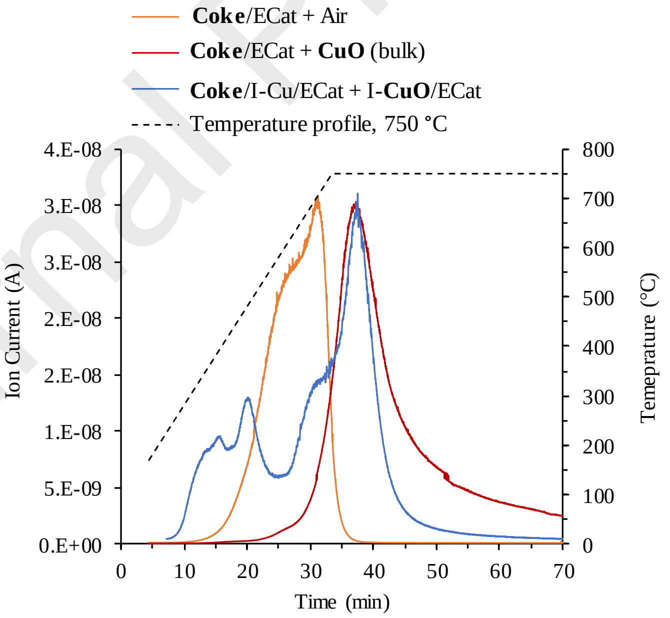

Figure 10. Combustion behaviour of coke using air, bulk-CuO, and I-CuO/ECat at 750 °C.

As required in the proposed CLC-FCC concept, the coke deposited on I-Cu/ECat and I-Mn_3O_4/ECat was successfully regenerated using the stoichiometrically required amount of oxidised oxygen carrier impregnated ECat (I-CuO/ECat and I-Mn_2O_3/ECat) at temperatures of 750 and 800 °C for 45 min, respectively. Siriwardane et al. [43] noticed that there were no significant effect on the CLC reaction of coal with CuO under N_2 or CO_2 which means that the results obtained here will also to the proposed CLC-FCC concept where the fluidisation gas in the regenerator must be CO_2 instead of air or N_2. The CLC tests were investigated under a temperature profile having a heating rate of 20 °C/min but, in reality, the coke deposited on FCC catalysts encounters high temperatures of *ca*. 750 °C when it is circulated to the regenerator. The regeneration time for the coke (deposited on reduced oxygen carriers modified ECat) with oxygen carriers is, therefore, likely to be shorter than the values observed in this study. Furthermore, in terms of coke combustion impregnation of CuO and Mn_2O_3 on FCC catalyst demonstrated much better results than the mechanically mixing of bulk-CuO.

4. Conclusions

The impregnation of Cu, MnO and Mn_3O_4 on ECat (I-Cu/ECat, I-MnO/ECat and I-Mn_3O_4/ECat) was shown to have few negative impacts on the cracking of n-hexadecane in terms of the conversion, yields, and product selectivities when compared with the reference ECat, as required for the proposed CLC-FCC concept. However, the impregnation of CoO on ECat (I-CoO/ECat) caused a decrease in the conversion of n-hexadecane. In terms of the CLC of coke deposited on FCC catalyst, the decomposition of oxidised oxygen carriers at lower temperatures was enhanced using the impregnation of CuO and Mn_2O_3 on the commercial ECat. Thanks to this enhancement, it was able to reach a high combustion efficiency at 750 °C, as used in commercial regenerators. The CLC tests of coke deposited on I-Cu/ECat and I-Mn_3O_4/ECat with stoichiometrically required amount of I-CuO/ECat and I-Mn_2O_3/ECat demonstrated that it is possible to reach about 90 vol. % combustion in FxB-MS and greater than 94 vol. % in FsB-MS at 750 °C for 45 min. The conditions (temperature and residence time) are the similar to those used in the conventional regenerator of FCC units, and so suggest that CLC is a promising technology to incorporate into the next generation of FCC units to optimise CO_2 capture.

Acknowledgements

The authors thank the University of Nottingham, Nanoscale and Microscale Research Centre (nmRC) for providing access to SEM instrumentation.

References

[1] EPA, Available and emerging technologies for reducing GHG emissions from petroleum refining, U.S. Environmental Protection Agency, 2010.

[2] J. van Straelen, F. Geuzebroek, N. Goodchild, G. Protopapas, L. Mahony, CO_2 capture for refineries, a practical approach, International Journal of Greenhouse Gas Control 4 (2010) 316-320.

[3] A. Elkamel, M. Ba-Shammakh, P. Douglas, E. Croiset, An optimization approach for integrating planning and CO_2 emission reduction in the petroleum refining industry, Industrial & Engineering Chemistry Research 47 (2008) 760-776.

[4] P. Peng, Y. Zhuang, The evaluation and comparison of carbon dioxide capture technologies applied to FCC flue gas, Advanced Materials Research, Trans Tech Publ, 2012, pp. 1479-1482.

[5] R. Digne, F. Feugnet, A. Gomez, A Technical and Economical Evaluation of CO_2 Capture from Fluidized Catalytic Cracking (FCC) Flue Gas, Oil & Gas Science and Technology–Revue d'IFP Energies nouvelles 69 (2014) 1081-1089.

[6] I. Miracca, D. Butler, CO_2 capture from a fluid catalytic cracking unit: Technical/Economical evaluation, in: K.F. Gerdes (Ed.) Carbon dioxide capture for storage in deep geologic formations, CPL Press, 2015, pp. 67-81.

[7] L.F. de Mello, R.D. Pimenta, G.T. Moure, O.R. Pravia, L. Gearhart, P.B. Milios, T. Melien, A technical and economical evaluation of CO_2 capture from FCC units, Energy Procedia 1 (2009) 117-124.

[8] T. Melien, S. Brown-Roijen, Economics, in: E. Lars (Ed.) Carbon dioxide capture for storage in deep geologic formation-Results from the CO_2 capture project., CPL Press2009, pp. 237-264.

[9] L.F. de Mello, R. Gobbo, G.T. Moure, I. Miracca, Oxy-combustion technology development for fluid catalytic crackers (FCC)–large pilot scale demonstration, Energy procedia 37 (2013) 7815-7824.

[10] L.F. de Mello, R. Gobbo, G.T. Moure, I. Miracca, CO_2 capture from a fluid catalytic cracking unit, in: K.F. Gerdes (Ed.) Carbon dioxide capture for storage in deep geologic formations-Results from the CO_2 capture project, CPL Press, 2015, pp. 47-49.

[11] L.F. de Mello, R. Gobbo, G.T. Moure, I. Miracca, FCC oxy-fuel demonstration at petrobras shale industrial business unit, in: K.F. Gerdes (Ed.) Carbon dioxide capture for storage in deep geologic formations-Results from the CO_2 capture project, CPL Press, 2015, pp. 51-65.

[12] F. Güleç, W. Meredith, C.-G. Sun, C.E. Snape, A novel approach to CO_2 capture in Fluid Catalytic Cracking—Chemical Looping Combustion, Fuel 244 (2019) 140-150.

[13] M. Crombie, S. Imbus, I. Miracca, CO_2 capture project phase 3—Demonstration phase, Energy Procedia 4 (2011) 6104-6108.

[14] E. Ksepko, R.V. Siriwardane, H. Tian, T. Simonyi, M. Sciazko, Effect of H_2S on chemical looping combustion of coal-derived synthesis gas over Fe–Mn oxides supported on sepiolite, ZrO_2, and Al_2O_3, Energy & Fuels 26 (2012) 2461-2472.

[15] A. Abad, M. de Las Obras-Loscertales, F. García-Labiano, L. de Diego, P. Gayán, J. Adánez, In situ gasification Chemical-Looping Combustion of coal using limestone as oxygen carrier precursor and sulphur sorbent, Chemical Engineering Journal 310 (2017) 226-239.

[16] H.R. Kerr, Capture and Separation Technology Gaps and Priority Research Needs, in: D.C. Thomas, S.M. Benson (Eds.) Carbon dioxide capture for storage in deep geologic formationse results from the CO_2 capture project, Elsevier, Oxford, UK, 2005.

[17] P. Gayán, A. Abad, L. De Diego, F. García-Labiano, J. Adánez, Assessment of technological solutions for improving chemical looping combustion of solid fuels with CO_2 capture, Chemical engineering journal 233 (2013) 56-69.

[18] T. Pröll, P. Kolbitsch, J. Bolhàr-Nordenkampf, H. Hofbauer, A novel dual circulating fluidized bed system for chemical looping processes, AICHE journal 55 (2009) 3255-3266.

[19] T. Mattisson, A. Lyngfelt, H. Leion, Chemical-looping with oxygen uncoupling for combustion of solid fuels, International Journal of Greenhouse Gas Control 3 (2009) 11-19.

[20] F. Gallucci, H. Hamers, M. van Zanten, M. van Sint Annaland, Experimental demonstration of chemical-looping combustion of syngas in packed bed reactors with ilmenite, Chemical Engineering Journal 274 (2015) 156-168.

[21] T. Drage, A. Arenillas, K. Smith, C. Snape, Comparison of pre and postcombustion CO_2 adsorbent technologies, 8th International Conference on Greenhouse Gas Control Technologies, 2006, pp. 19-22.

[22] L.F. de Mello, G.T. Moure, O.R. Pravia, L. Gearhart, P.B. Milios, Oxy-combustion for CO_2 capture from fluid catalytic crackers (FCC) in: E. Lars (Ed.) Carbon dioxide capture for storage in deep geologic formation-Results from the CO2 capture project, CPL Press2009, pp. 31-42.

[23] A. Corma, L. Sauvanaud, M. Occellli, Fluid Catalytic Cracking VII: Materials, Methods and Process Innovations, Elsevier, BV, Ámsterdam (2007).

[24] J. Barker, P. Richards, C. Snape, W. Meredith, A novel technique for investigating the nature and origins of deposits formed in high pressure fuel injection equipment, SAE International Journal of Fuels and Lubricants 2 (2010) 38-44.

[25] ASTM, Standard Test Method for Testing Fluid Catalytic Cracking (FCC) Catalysts by Microactivity Test, D3907-13ASTM International, 2013.

[26] M. Thommes, K. Kaneko, A.V. Neimark, J.P. Olivier, F. Rodriguez-Reinoso, J. Rouquerol, K.S. Sing, Physisorption of gases, with special reference to the evaluation of surface area and pore size distribution (IUPAC Technical Report), Pure and Applied Chemistry 87 (2015) 1051-1069.

[27] K. Sing, Reporting physisorption data for gas/solid systems with special reference to the determination of surface area and porosity (Provisional), Pure and applied chemistry 54 (1982) 2201-2218.

[28] S. Wang, Q. Cai, J. Chen, L. Zhang, L. Zhu, Z. Luo, Co-cracking of bio-oil model compound mixtures and ethanol over different metal oxide-modified HZSM-5 catalysts, Fuel 160 (2015) 534-543.

[29] C. Li, J. Ma, Z. Xiao, S.B. Hector, R. Liu, S. Zuo, X. Xie, A. Zhang, H. Wu, Q. Liu, Catalytic cracking of Swida wilsoniana oil for hydrocarbon biofuel over Cu-modified ZSM-5 zeolite, Fuel 218 (2018) 59-66.

[30] K. Kubo, H. Iida, S. Namba, A. Igarashi, Comparison of steaming stability of Cu-ZSM-5 with those of Ag-ZSM-5, P/H-ZSM-5, and H-ZSM-5 zeolites as naphtha cracking catalysts to produce light olefin at high temperatures, Applied Catalysis A: General 489 (2015) 272-279.

[31] O. Awayssa, N. Al-Yassir, A. Aitani, S. Al-Khattaf, Modified HZSM-5 as FCC additive for enhancing light olefins yield from catalytic cracking of VGO, Applied Catalysis A: General 477 (2014) 172-183.

[32] Z. Du, X. Ma, Y. Li, P. Chen, Y. Liu, X. Lin, H. Lei, R. Ruan, Production of aromatic hydrocarbons by catalytic pyrolysis of microalgae with zeolites: Catalyst screening in a pyroprobe, Bioresource technology 139 (2013) 397-401.

[33] K. Kubo, H. Iida, S. Namba, A. Igarashi, Ultra-high steaming stability of Cu-ZSM-5 zeolite as naphtha cracking catalyst to produce light olefin, Catalysis Communications 29 (2012) 162-165.

[34] F. Güleç, W. Meredith, C.-G. Sun, C.E. Snape, Selective low temperature chemical looping combustion of higher alkanes with Cu-and Mn-oxides, Energy 173 (2019) 658-666.

[35] T.B. Siregar, N. Amin, Catalytic cracking of palm oil to gasoline over pretreated Cu-ZSM-5, Jurnal Teknologi 44 (2006).

[36] N. Hosseinpour, Y. Mortazavi, A.A. Khodadadi, Cumene cracking activity and enhanced regeneration of FCC catalysts comprising HY-zeolite and $LaBO_3$ (B= Co, Mn, and Fe) perovskites, Applied Catalysis A: General 487 (2014) 26-35.

[37] W.B. Widayatno, G. Guan, J. Rizkiana, J. Yang, X. Hao, A. Tsutsumi, A. Abudula, Upgrading of bio-oil from biomass pyrolysis over Cu-modified β-zeolite catalyst with high selectivity and stability, Applied Catalysis B: Environmental 186 (2016) 166-172.

[38] C.L. Koon, F. Akbar, R. Hughes, Y.R. Tyagi, M.C. Diaz, S.C. Martin, P.J. Hall, and C.E. Snape, Development of an experimental protocol to evaluate FCC stripper performance in terms of coke yield and composition, Chemical Engineering Research and Design, 78(5) (2000) 738-744.

[39] B. Behera, P. Gupta, S.S. Ray, Structure and composition of hard coke deposited on industrial fluid catalytic cracking catalysts by solid state 13 C nuclear magnetic resonance, Applied Catalysis A: General 466 (2013) 123-130.

[40] A. Voorhies, Carbon formation in catalytic cracking, Industrial & Engineering Chemistry 37 (1945) 318-322.

[41] A. Shabani, M. Rahman, D. Pudasainee, A. Samanta, P. Sarkar, R. Gupta, Evaluation of ash-free coal for chemical looping combustion-part I: Thermogravimetric single cycle study and the reaction mechanism, The Canadian Journal of Chemical Engineering 95 (2017) 623-633.

[42] J. Adanez, A. Abad, F. Garcia-Labiano, P. Gayan, F. Luis, Progress in chemical-looping combustion and reforming technologies, Progress in Energy and Combustion Science 38 (2012) 215-282.

[43] R. Siriwardane, H. Tian, G. Richards, T. Simonyi, J. Poston, Chemical-looping combustion of coal with metal oxide oxygen carriers, Energy & Fuels 23 (2009) 3885-3892.

Highlights:

- Demonstrated the applicability of CLC for the regeneration of FCC catalyst
- Developed a new generation of FCC catalyst containing Mn- and Cu-based oxygen carriers
- Impregnation of Cu/ECat and Mn_3O_4/ECat did not negatively affect cracking reaction
- > 94 wt.% combustion of coke achieved with CuO and Mn_2O_3 impregnated ECat at 750 °C

Demonstrating the applicability of chemical looping combustion for the regeneration of fluid catalytic cracking catalysts

Fatih Güleç*, Will Meredith, Cheng-Gong Sun, Colin E Snape

University of Nottingham, Faculty of Engineering, Energy Technologies Building, Triumph Road, Nottingham NG7 2TU, UK. *Fatih.Gulec@nottingham.ac.uk

Appendix A. Characterization of reduced oxygen carriers impregnated ECat before and after cracking

X-ray diffraction (XRD) analysis:

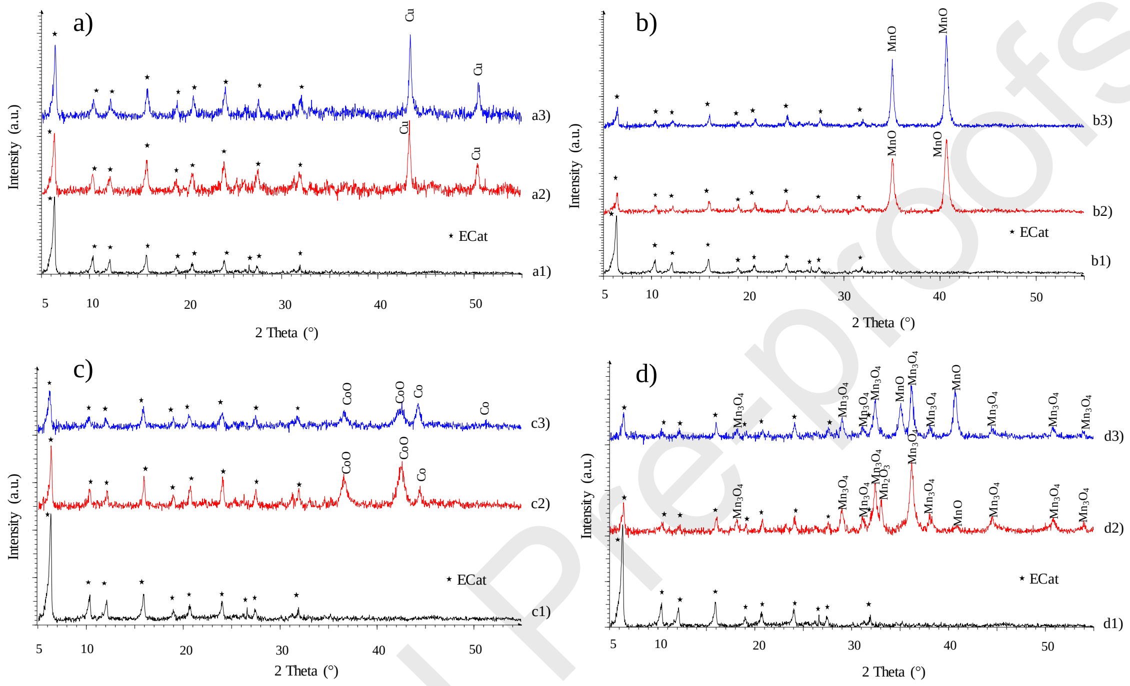

Figure A1. XRD patterns of a) I-Cu/ECat, b) I-MnO/ECat, c) I-CoO/ECat and d) I–Mn_3O_4/ECat (patters; “1” ECat, “2” fresh reduced oxygen carriers impregnated ECat, and “3” used reduced oxygen carriers impregnated ECat after cracking reaction).

X-ray fluorescence (XRF) analysis:

Table A1. Proportion of reduced oxygen carriers impregnated with ECat.

Catalyst	True density[a] (g/cm^3)	Theoretical loading[b] (wt.%)	Actual loading[c] (wt.%)
ECat	2.70	-	-
I-Cu/ECat	2.77	5.4	6.6
I-CoO/ECat	2.94	16.8	16.3
I-Mn_3O_4/ECat	3.05	29.0	29.4
I-MnO/ECat	3.09	27.7	26.7

[a] Measured by Helium Pycnometer. [b] Determined the reduced oxygen carriers based on the weight differences of ECat before and after oxygen carrier impregnation and reduction. [c] Determined the reduced oxygen carriers using XRF.

Scanning electron microscope (SEM) analysis:

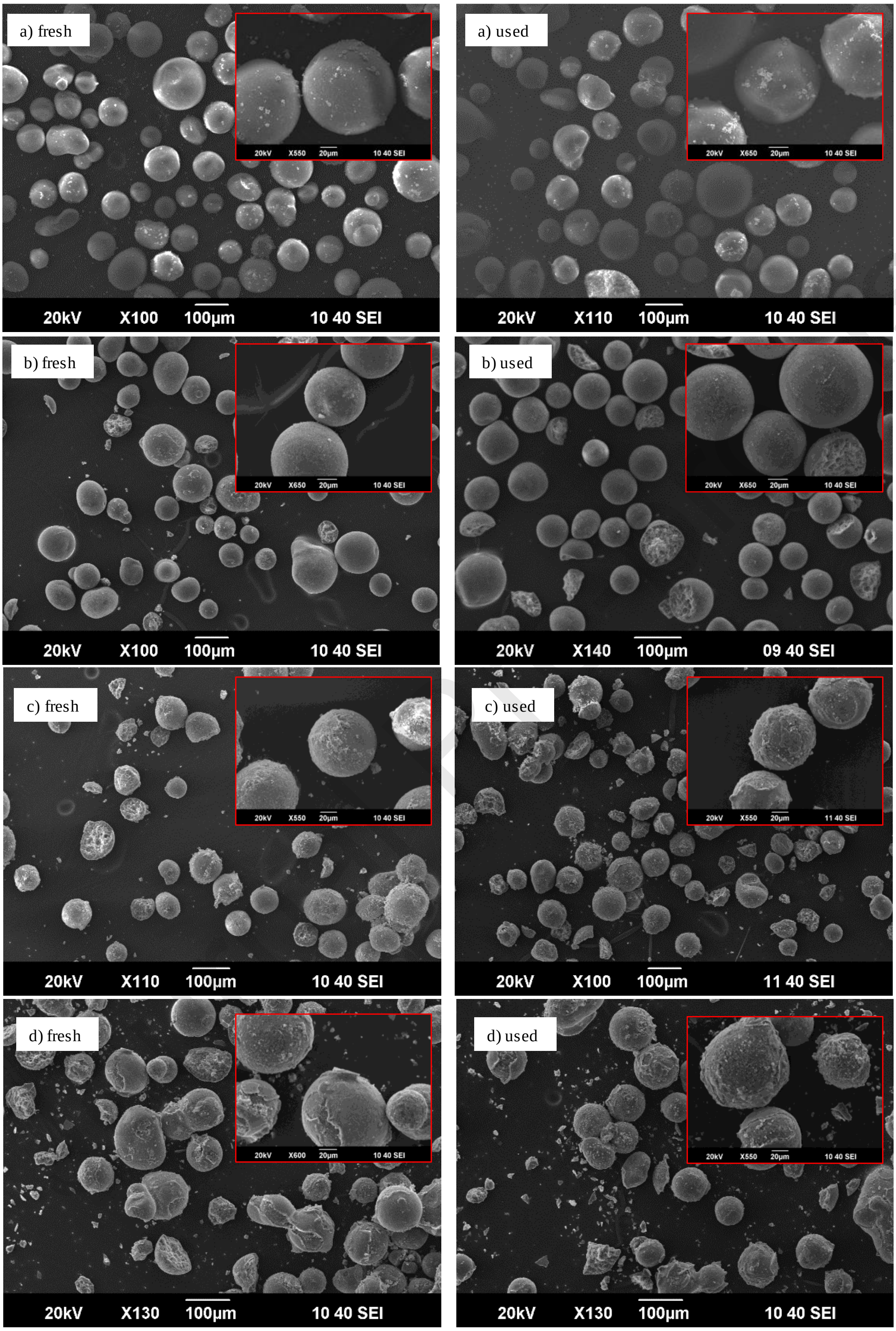

Figure A2. SEM images of a) I-Cu/ECat, b) I-CoO/ECat c) I–Mn_3O_4/ECat and d) I-MnO/ECat (fresh: reduced oxygen carriers impregnated ECat after reduction of oxidised oxygen carriers by hydrogen, used: reduced oxygen carriers impregnated ECat after cracking reaction).

N_2 adsorption-desorption analysis:

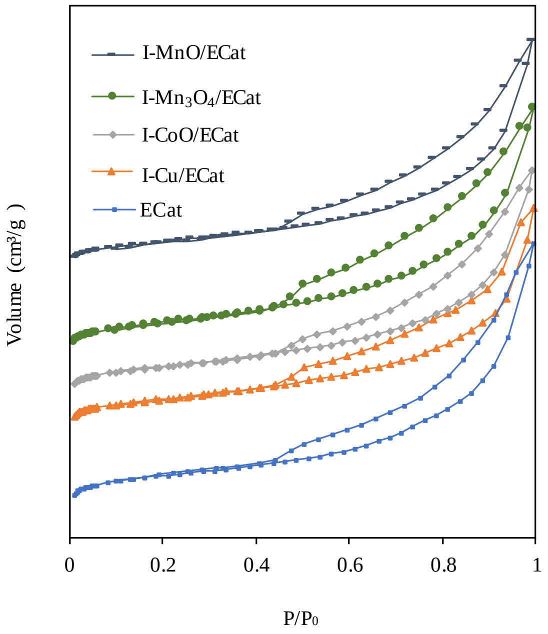

Figure A3. Nitrogen adsorption-desorption isotherms of fresh reduced oxygen carriers impregnated ECat; ECat, I-Cu/ECat, I-CoO/ECat, I-Mn_3O_4/ECat, I-MnO/ECat.

Table A2. Textural properties of ECat, I-Cu/ECat, I-CoO/ECat, I-Mn_3O_4/ECat, I-MnO/ECat.

Catalyst	Surface area (m^2/g)		Pore volume (cm^3/g)			Pore diameter (nm)[e]	
	S_{BET} [a]	S_{micro} [b]	V_{tot} [c]	V_{meso} [d]	V_{micro} [b]	d_{av}	d_{neck}
ECat	191	102	0.25	0.20	0.05	13.8	11.0
I-Cu/ECat	179	116	0.19	0.15	0.04	13.0	10.3
I-CoO/ECat	181	103	0.19	0.16	0.03	13.5	10.2
I-Mn_3O_4/ECat	169	74	0.17	0.15	0.02	12.8	8.8
I-MnO/ECat	177	87	0.18	0.17	0.01	13.7	10.0

[a] The BET surface area (S_{BET}) was calculated on the basis of g ECat. [b] Micro surface area (S_{micro}) and pore volume (V_{micro}) were calculated using the t-Plot method. [c] Total pore volume (V_{tot}) was calculated by the BJH method. [d] Meso-pore volume (V_{meso}) was calculated by differences of total and micro-pore volumes. [e] Pore diameters, average (d_{av}) and neck (d_{neck}), were calculated by BJH method.

The nitrogen sorption isotherms and textural properties of reduced oxygen carrier modified ECat, I-Cu/ECat, I-CoO/ECat, I-Mn_3O_4/ECat, and I-MnO/ECat, are presented in Figure A3 and Table A2. The impregnation of reduced oxygen carriers did not change the sorption isotherms of ECat, which are defined as “type IV” according to International Union of Pure and Applied Chemistry (IUPAC) classification [1, 2]. The isotherms consisted of two well-distinguished regions; adsorption of monolayer-multilayer and capillary condensation. The initiation part of the isotherms (P/P_0 = 0-0.4) are attributed to the former; monolayer-multilayer adsorption [1, 2]. Additionally the characteristic hysteresis is usually attributed to the latter (P/P_0 = 0.4-1.0), capillary condensation, taking place in mesoporous [1]. Pore condensation is defined as a gas condensation to a liquid-like phase in the pore at a pressure, P, less than the saturation pressure, P_0, of bulk liquid [1]. Furthermore, the hysteresis loops are mainly classified as four types and the hysteresis drawn for the prepared catalyst s can be defined as “type H3” [1, 2]. The common features of type H3 loop are the sharp step down of the desorption branch which is generally located in a narrow range P/P_0 (~0.4-0.5) for the particular adsorptive and temperature (nitrogen at temperatures of 77 K) [1].

Acidity via Fourier-transform infrared spectroscopy of pyridine adsorption (Py-IR):

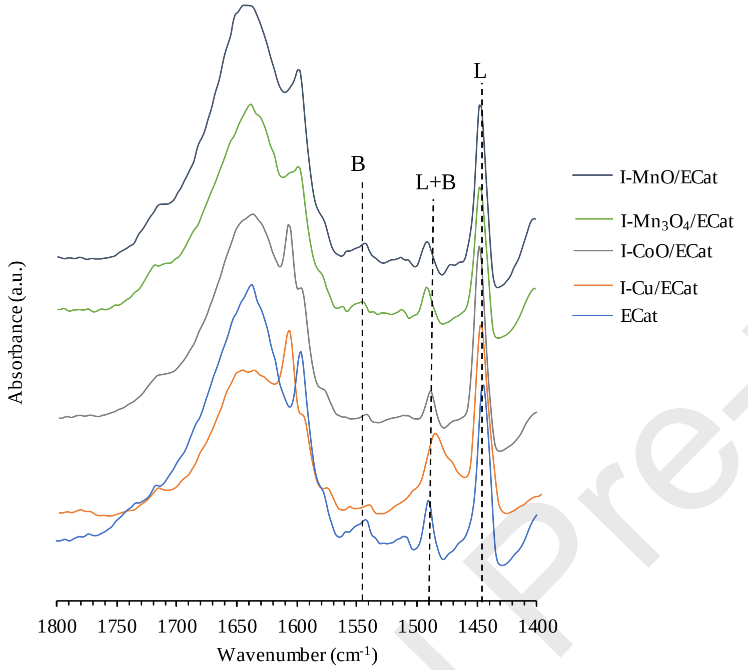

Figure A4. FTIR of adsorbed pyridine for parent and reduced form oxygen carrier impregnated ECat.

Table A3. The integrated area of FTIR graph for the pyridine adsorbed parent and reduced form oxygen carrier impregnated ECat (presented in arbitrary unit - a.u.).

Catalyst	L[a] (1445 cm^{-1})	L or B (1490 cm^{-1})	B[b] (1545 cm^{-1})	B/L
ECat	0.76	0.15	0.10	0.13
I-Cu/ECat	0.65	0.37	0.04	0.06
I-CoO/ECat	0.72	0.16	0.01	0.01
I-Mn_3O_4/ECat	0.57	0.10	0.04	0.07
I-MnO/ECat	0.68	0.08	0.08	0.11

[a] Lewis (L) acidity area measured by IR peak at 1445 cm^{-1}. [b] Brönsted (B) acidity area measured by IR peak at 1545 cm^{-1}.

The Brönsted (B) and Lewis (L) acidities measured by Py-IR of parent ECat and reduced oxygen carriers impregnated ECat, I-Cu/ECat, I-CoO/ECat, I-Mn_3O_4/ECat, and I-MnO/ECat, are presented in Figure A4 and the integrated area of the peaks are summarized in Table A3 as arbitrary unit. The interactions of pyridine-Brönsted and pyridine-Lewis acid sites are indicated with a group of adsorption bands on the FTIR spectrum, at 1540 and 1640 cm^{-1} (Brönsted acidity [3]), at 1445, 1580 and 1620 cm^{-1} (Lewis acidity [3, 4]) and the band about 1490 cm^{-1} (either Lewis or Brönsted acidity [3-5]).

Appendix B. CLC of model and real FCC coke with bulk oxygen carriers

Calibration graph for the converting ion current to percentage of CO_2 in combustion gases mixtures: Thanks to the calibration graphs (Figure B1), the Ion Currents measured by MS with time could be converted to the volumetric CO_2 percentage in the output gas mixture. It is, therefore, able to calculate the volumetric flow rate of CO_2 in time using a constant carrier gas flow rate of N_2.

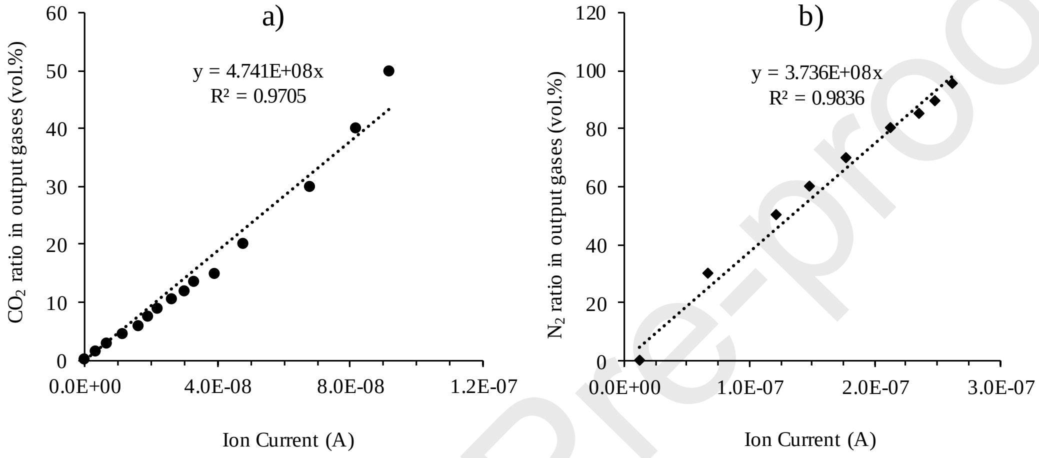

Figure B1. Calibration graph for the conversion of measured ion current (A) to a) vol. % of CO_2 and b) vol. % of N_2 in combustion gases mixture.

References

[1] M. Thommes, K. Kaneko, A.V. Neimark, J.P. Olivier, F. Rodriguez-Reinoso, J. Rouquerol, K.S. Sing, Physisorption of gases, with special reference to the evaluation of surface area and pore size distribution (IUPAC Technical Report), Pure and Applied Chemistry 87 (2015) 1051-1069.

[2] K. Sing, Reporting physisorption data for gas/solid systems with special reference to the determination of surface area and porosity (Provisional), Pure and applied chemistry 54 (1982) 2201-2218.

[3] F. Hernández-Beltrán, R. Quintana-Solórzano, J. Sánchez-Valente, F. Pedraza-Archila, F. Figueras, Effect of highly reactive sulfur species on sulfur reduction in cracking gasoline, Applied Catalysis B: Environmental 42 (2003) 145-154.

[4] V.S. Marakatti, G.V. Shanbhag, A. Halgeri, Sulfated zirconia; an efficient and reusable acid catalyst for the selective synthesis of 4-phenyl-1, 3-dioxane by Prins cyclization of styrene, Applied Catalysis A: General 451 (2013) 71-78.

[5] O. Awayssa, N. Al-Yassir, A. Aitani, S. Al-Khattaf, Modified HZSM-5 as FCC additive for enhancing light olefins yield from catalytic cracking of VGO, Applied Catalysis A: General 477 (2014) 172-183.